Article:
He, X, Lou, T, Cao, P et al. (4 more authors) (2021) Experimental and molecular dynamics simulation study of chemically stable superhydrophobic surfaces. Surface and Coatings Technology, 418. 127236. ISSN 0257-8972

https://doi.org/10.1016/j.surfcoat.2021.127236

Experimental and molecular dynamics simulation study of chemically stable superhydrophobic surfaces

Xiaoyan He [a,b], Tong Lou [a], Pan Cao [c], Xiuqin Bai [a,&], Chengqing Yuan [a], Chun Wang [b], Anne Neville [b]

[a] Reliability Engineering Institute, National Engineering Research Center for Water Transport Safety, Wuhan University of Technology, Wuhan 430063, China

[b] Institute of Functional Surfaces, School of Mechanical Engineering, University of Leeds, Leeds LS2 9JT, United Kingdom

[c] College of Mechanical Engineering, Yangzhou University, Yangzhou 255127, China

[&] Corresponding author.

E-mail address: xqbai@whut.edu.cn

ABSTRACT

Experimental and molecular dynamics simulation study were used to clarify the hydrophilicity of substrate surfaces and hydrophobicity of as-prepared surfaces at molecular level. First, an easy one-step approach was utilized to construct superhydrophobic surfaces on different substrates such as steel, aluminum, glass, and silicon wafer. The superhydrophobicity of as-prepared surfaces were contributed to the fluorinated compositions and microstructures. A fluorinated surface was constructed as a model of the as-prepared superhydrophobic surface. Molecular dynamics simulations were utilized to elucidate the anti-wetting mechanism of as-prepared fluorinated surfaces on aluminum substrates. Compared with the compact hydrated layer on the aluminum substrate, the hydrated layer on the fluorinated surface were broader with a lower intensity, confirming the lower attractive force between surface and water molecules. The decreased van der Waals interaction with water molecules contributed to the hydrophobicity of the fluorinated surface. while, in an alkaline solution, the electrostatic interaction had a negative impact on hydrophobicity of a fluorinated surface.

Keywords: Superhydrophobicity; various substrates; chemical stability; molecular dynamics simulation; molecular interaction

1. Introduction

Highly functional superhydrophobic surfaces widely exist in nature [1, 2]. Inspired by these fascinating phenomenon, superhydrophobic surfaces, with the water contact angle higher than 150° and the contact angle hysteresis lower than 5°, have been developed rapidly [3-5]. Superhydrophobic surfaces possess special interfacial behavior and are widely applied in various applications, including self-cleaning [6, 7], anti-icing [8], antifouling [9, 10], anticorrosion [11, 12], and anti-drag [13, 14].

In general, surface heterogeneity and roughness are the major factors responsible for superhydrophobicity of surfaces [15, 16]. Low-surface-energy materials and micro/nanostructures are usually combined to obtain superhydrophobic surfaces [17]. Conventionally, there are mainly two ways to achieve superhydrophobic surfaces: fabrication of a rough surface on a hydrophobic material, or modification of hydrophobic materials on a rough surface [18]. Until now, numerous methods have been used to construct superhydrophobic surfaces, including laser ablation [19], sol-gel methods [20], phase separation [21], and chemical etching [22, 23]. In these traditional methods, rough surfaces were first obtained, and then low-surface-energy materials were modified to construct superhydrophobic surfaces. Schlaich et al. [3] prepared superhydrophobic surfaces by modification fatty acid chloride onto hierarchical surfaces. Gao et al. [22] obtained superhydrophobic surfaces via etching in H_2SO_4/H_2O_2 solution and followed by modification with low surface energy material. Peng et al. [24] proposed a two-step process to obtain a superamphiphobic aluminum surface, involving the construction of micro/nanoscale structure and fluorination treatment. Zhang et al. [25] fabricated robust superhydrophobic SiO_2/ polydimethylsiloxane films by sol-gel process and subsequent modification of polydimethylsiloxane. All these studies usually involved two steps and stressed the importance of the combination of hydrophobic materials and rough surfaces in the construction of superhydrophobic surfaces. If both hydrophobicity and roughness of surface could be obtained in just one step, the traditional two-step methods to fabricate superhydrophobic surfaces could be replaced.

Saleema et al. [26] prepared superhydrophobic surfaces by a simple one-step process, where aluminum substrates were immersed in a mixed solution containing NaOH and fluoroalkyl-silane. The chemical reaction between NaOH and aluminum contributed to

the rough microporous surface. Simultaneously, the adsorption of fluoroalkyl-silane molecules onto the newly formed microporous surface led to a low surface energy. The incorporation of a rough microporous surface and hydrophobic molecules contributed to the construction of superhydrophobic surfaces. Zhang et al. [27] prepared superhydrophobic surfaces on aluminum substrates by electrodeposition in manganese (II) chloride tetrahydrate and stearic acid ethanol solution. The adsorption of stearic acid during the formation of hierarchical structures, resulted in the superhydrophobic surfaces by one-step process. These one-step methods used to fabricate superhydrophobic surfaces are limited to certain substrates. It is meaningful to develop a simple method which is also suitable for a wide range of substrates to obtain superhydrophobic surfaces without specialized equipment. Meanwhile, most of superhydrophobic surfaces lose their antiwetting properties when they are in strong acid/alkali solutions [24, 27]. It is also worthwhile to promote their chemical stability toward solutions with different pH.

The interaction between the liquid and the solid surface could help to understand their special wettability. At present, some researches have been focused on the interactions between droplets and solid surfaces by molecular dynamics (MD) simulations [28-31]. Zhang et al. studied the wetting process of water molecules on coal surface with varying coalification [29]. Guo et al. investigated water droplet morphology and mobility on liquid infused surfaces, which could help to better understand their thermodynamically stable states [32]. MD simulations could provide significant guidelines to understanding the wetting behavior. While, these studies were focused on deionized water, the interactions between the liquids with different pH and solid surfaces are still poorly understood.

The study aimed at fabricating superhydrophobic surfaces by an easy one-step sol-gel process which is compatible with various materials such as steel, aluminum, glass, and silicon wafer substrates. The superhydrophobic surfaces were fabricated by soaking the substrates into a titanium butoxide and (1H,1H,2H,2H-perfluorodecyl)-triethoxysilane (PFTEOS) mixed solution. The adsorption of PFTEOS molecules on the newly assembled titania surfaces led to the successful fabrication of superhydrophobic surfaces. MD simulations were utilized to investigate the interaction between HCl/NaOH solution and the solid surface to provide further understanding of surface

wettability.

2. Experimental Details

2.1. Fabrication of superhydrophobic samples

Type 316L stainless steel substrates, aluminum substrates, silicon wafers and glass substrates were used in this study. 316L stainless steel substrates and aluminum substrates were polished, washed with deionized water and subsequently dried in a vacuum. 98% sulfuric acid and 30% hydrogen peroxide were mixed in 7:3 volumetric ratio to prepare a piranha solution. 316L stainless steel substrates, silicon wafers and glass substrates were immersed into the fresh piranha solution for 30 minutes at 85 °C to create hydroxyl groups. Aluminum substrates were activated by UV irradiation to generate hydroxyl groups.

A sol-gel deposition process was used to deposit superhydrophobic titanium oxide multilayer coatings on various substrates. Briefly, the substrates were immersed into an ethanol solution containing 0.1 M titanium butoxide and 0.1 M (1H,1H,2H,2H-perfluorodecyl)-triethoxysilane (PFTEOS) for a period of time. The samples were washed by ethanol three times to remove unbound molecules and then hydroxyl groups were recreated by immersion in deionized water for 2 minutes, subsequently drying in an air stream. The steps were repeated to prepare multilayers to form titania coatings modified by PFTEOS. The deposition times and deposition cycles were depended on the different substrates. After deposition, all the samples were washed by water and ethanol to remove the unreacted molecules and then dried in an oven at 120 ºC.

2.2. Characterization

A field emission scanning electron microscopy (FESEM, TESCAN VEGA3, Czech Republic) was used to observed surface morphologies of the samples. Coverage% was the ratio of the area of particles to the area of actual substratum surface, which was calculated by *ImageJ* software. The size distributions of particles were calculated by *Image Pro Plus* software. An energy-dispersive spectroscopy (EDS, Oxford, England) with an accelerating voltage of 10 kV was used to analysis elemental compositions of as-prepared coatings. Fourier transform infrared spectroscopy (FTIR, Nicolet AVATAR 360, USA) with a resolution of 4 cm^{-1} and a scan number of 8 was used to investigate functional groups on coatings. X-ray photoelectron spectroscopy (XPS, ESCALAB

250Xi, U.S.A) with Al-k_α (1486.6 eV) as radiation resource were further used to study their chemical compositions. The wettability of samples was evaluated by a contact angle meter (Dataphysics OCA 15EC, Germany). Contact angles were tested at different locations per sample by fitting water drops with the Laplace-Young equation.

2.3. Molecular dynamics (MD) simulation

All the molecular dynamics simulations were conducted by the Forcite program with COMPASS force-field [30, 33]. PFTEOS ($CF_3(CF_2)_7CH_2CH_2Si(OCH_2CH_3)_3$), with a long perfluorocarbon chain, usually strongly and stably binds with hydroxylated surfaces. Therefore, all the alkoxysilane branches in PFTEOS molecules were replaced by –OH groups through hydrolysis and their structure was simplified into $CF_3(CF_2)_7CH_2CH_2Si(OH)_3$ in this study as previous studies [34, 35]. PFTEOS could be the surface component of the as-prepared surface, which was used to construct the simulated fluorinated surface. The anatase TiO_2 (101) crystal plane is particularly chosen to represent the newly formed amorphous TiO_2 because of its stability compared with other crystal planes. The simulated fluorinated surface was constructed according to a previous report [29]. 16 $CF_3(CF_2)_7CH_2CH_2Si(OH)_3$ molecules were inserted near the titania surface with parameters of 27.21 Å × 26.43 Å, γ=110.3°, and an one-layer graphite sheets were placed on the side of the fluorinated layer along the Z-axis and their distance was adjusted as close as possible [29]. The graphite sheet and the TiO_2 (101) substrate were fixed to avoid transformation. After the system was geometrically optimized and equilibrated for 500 ps with NVT ensemble at 298 K, the graphite sheets were moved closer to the fluorinated layer, and the system was optimized again. The geometry optimization was repeated until the layer surface was smooth. Finally, the graphite sheet and TiO_2 (101) substrate were removed, and the system was relaxed by 500 ps dynamics to ensure the stability of the final structure. The optimization of the fluorinated layer was finished. Aluminum substrate was chosen for comparison since that it is sensitive to both acid and alkaline solutions. For comparison purpose, the stable Al (111) surface was particularly used with parameters of 28.63 Å × 28.63 Å × 7.01 Å, α=β=90°, γ=120°. For the simulated solution, a water layer with an area of 28.63 Å ×

28.63 Å (500 H_2O molecules) was built close to the Al (111) and fluorinated surfaces. 10 $H3O^+/Cl^-$ and 10 Na^+/OH^- ions were added to the water box to simulate acid solution and alkalic solution. The layered interface simulation model was successfully constructed with a vacuum layer of 20 Å. With geometrical optimization, the interface model reached a convergence state. After that, a dynamic simulation of the entire system was carried out for 500 ps with NVT ensemble, the Nosé-Hoover method as thermal bath, the temperature under 298 K, and 1 fs time step [30]. Results of the last 400 ps were adopted to analyze the properties.

3. Results and discussion

3.1 Synthesis of Titania Coatings

Titania coatings were prepared by repeating adsorption and subsequent hydrolysis of titanium butoxide and PFTEOS. The formation process of titania particles with grafting PFTEOS on substrates is depicted in Fig. 1. The process was composed of chemisorption and hydrolysis. Titanium butoxide and PFTEOS were simultaneously chemisorbed on hydroxylated surfaces when the hydroxylated surfaces were immersed in the titanium butoxide and PFTEOS mixed solution. The hydroxyl groups on the hydroxylated surface would induce the chemisorption of titanium butoxide [36]. The reaction between silane species in PFTEOS molecules and surface functional groups on hydroxylated surfaces lead to the formation of a monolayer with long perfluorocarbon chains [24, 37]. Titania particles with grafting PFTEOS were formed after hydrolysis of chemisorbed alkoxides and a silane coupling agent. The surfaces with alkoxide and silane coupling agent were then washed by ethanol to remove unbound alkoxides and then hydroxyl groups were regenerated by immersion in deionized water. The chemisorption and hydrolysis steps were repeated to form titania coatings (Fig. 1).

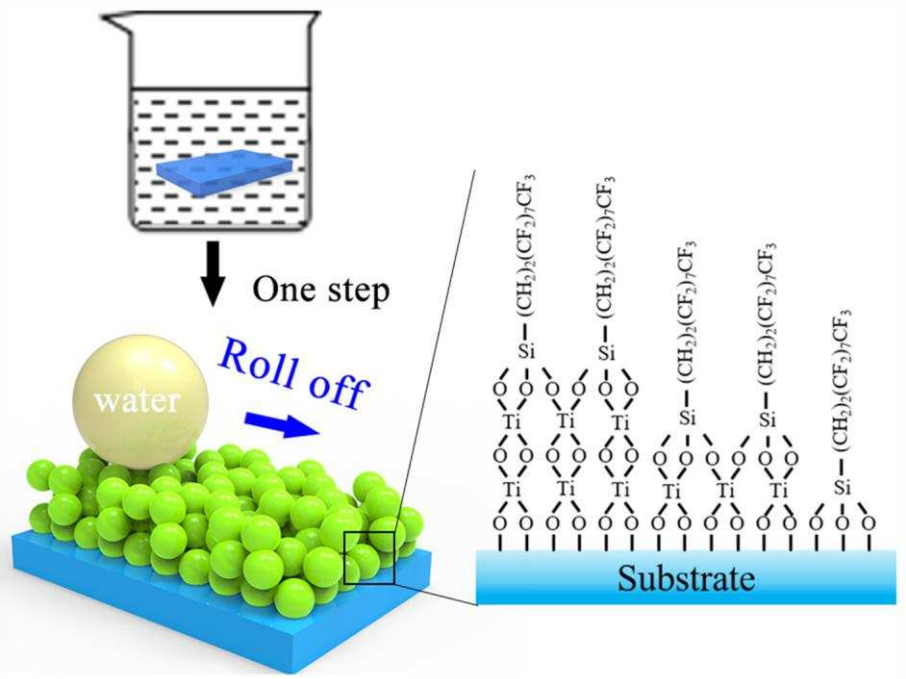

Fig. 1. Schematic diagrams illustrating the synthetic route of titania coatings with PFTEOS on hydroxylated surfaces via sol-gel deposition.

3.2 Characterization of As-Prepared Titania Coatings

The as-prepared titania coatings on silicon wafers after a deposition time of 30 minutes were characterized by EDS, FTIR and XPS analyses (Fig. 2). EDS spectrum shows that the as-prepared surfaces consist of C, O, F, Ti, and Si elements. Moreover, the atomic ratio of Ti and O is about 1:2, which is consistent with the atomic ratio of titania, suggesting successful formation of titania (Inset in Fig. 2a). The IR spectra indicate obvious peaks from PFTEOS. The peak at 3391 cm^{-1} is attributed to O−H stretching vibration and the peak located at 702 cm^{-1} is attributed to Ti−O−Ti stretching vibration [38]. The four peaks at 1232, 1199, 1145 and 1113 cm^{-1} imply the existence of $-CF_2$ and $-CF_3$ groups [39, 40]. The peak at 1062 cm^{-1} indicates the formation of Si−O bonds [39]. XPS examination provides further evidence of the successful formation of titania particles with grafted fluorine functional groups (Fig. 2c). The elements Ti, C, O, and F are also clearly seen in XPS spectra and their quantitative data is shown (Inset in Fig. 2c).

The high-resolution C *1s*, Ti *2p*, and F *1s* spectra further confirm the formation of titania with grafting PFTEOS molecules (Fig. 2 d, e, f). The Ti *2p* spectrum is attributed to three peaks at 459.2 eV, 464.9 eV and 471.8 eV, respectively (Fig. 2d). The peaks are

attributed to TiO_2 $2p_{3/2}$, TiO_2 $2p_{1/2}$ and their satellite peaks, respectively, which indicate the successful formation of titania particles. The C 1s spectrum is assigned to four components, namely CF_3 (292.8 eV), CF_2 (290.9 eV), C−O (287.7 eV) and C−C/C−H (284.8 eV) [26] (Fig. 2e). The F 1s spectrum reveals exist of $-CF_2$ (688.0 eV) and $-CF_3$ (690.1 eV) (Fig. 2f), indicating PFTEOS molecules binding with the titania particles. The C atomic concentrations of $-CF_3$, $-CF_2$ groups from the C 1s spectrum are about 20.75 at% and 42.20 at%, respectively. The ratio of CF_2/CF_3 is about 2, which is smaller than the theoretical value ~7 acquired from the molecular structure of PFTEOS, suggesting that the $-CF_3$ function groups comprise the outermost surface. Hydrophobic properties are attributed to the existence of $-CF_2/-CF_3$ groups and $-CF_3$ functional groups in the outermost surface.

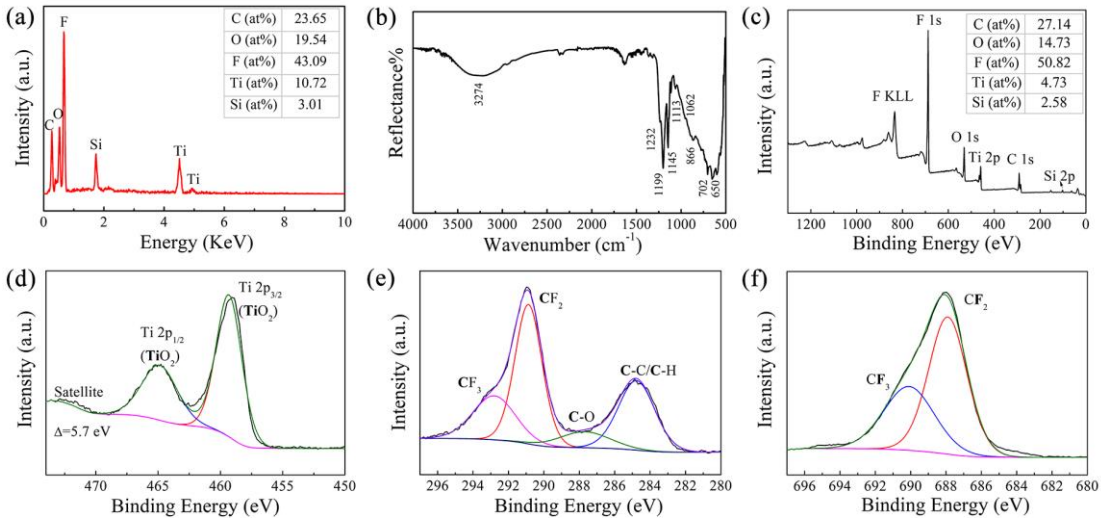

Fig. 2. EDS (a), FTIR (b), XPS (c), Ti *2p* (d), C *1s* (e), and F *1s* (f) spectra detected from as-prepared titania coatings (Insets are quantitative analysis results from EDS and XPS, respectively)

Titania coatings on silicon wafers prepared with different deposition times are exhibited in Fig. 3, suggesting that titania coatings are successfully constructed on silicon wafers. An increase in particle number and film density with increasing deposition times is visible (Fig. 3b), highlighting the importance of deposition times. Meanwhile, aggregates of titania particles are clearly observed, which might be due to destabilization of titanium butoxide. The titania particles nearby tend to aggregate due to their high surfactivity at nanoscale [41]. Larger titania particles are formed on these coatings, indicating that the deposition times directly impact particle sizes (Fig. 3c). That means the total roughness and thickness of the as-prepared coatings can be

adjusted by changing the deposition times.

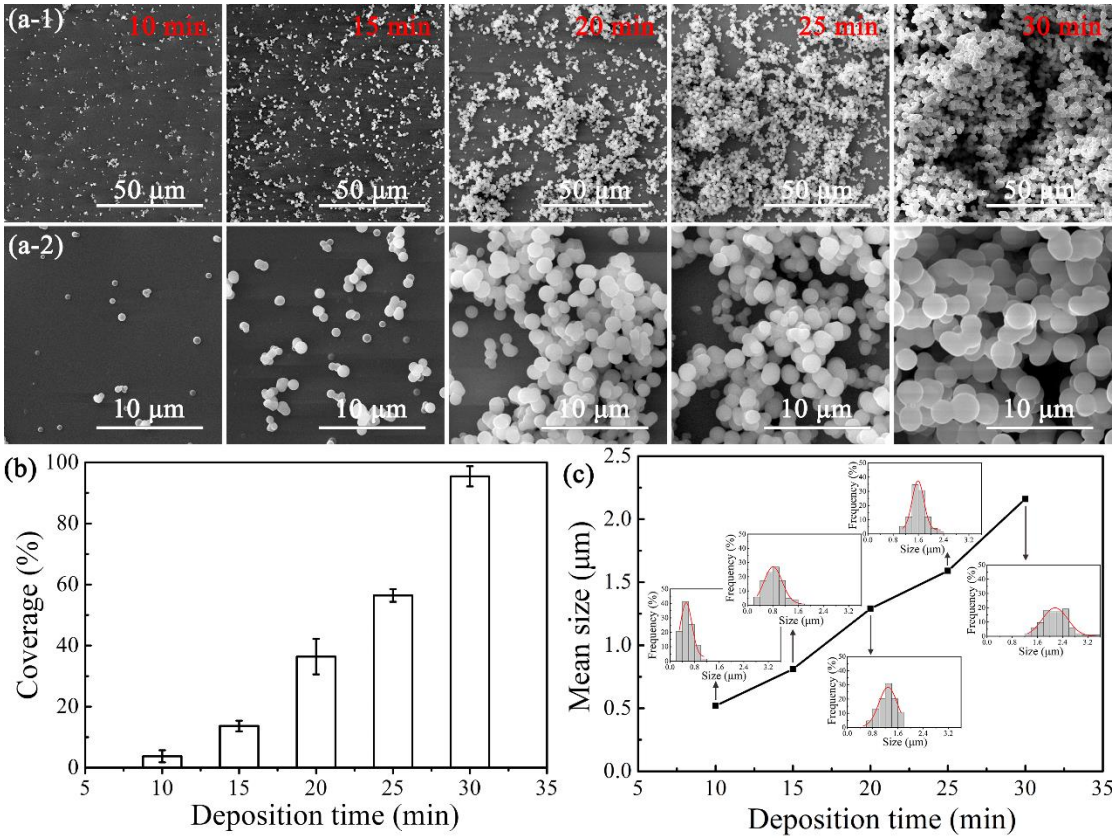

Fig. 3. Characterization of titania coatings on silicon wafers. (a) SEM images after different deposition times, respectively. (b) Increase in surface coverage after different deposition times. (c) Increase in mean sizes of particles after different deposition times.

The wettability of the coatings with different deposition times was quantified by water contact angle and contact angle hysteresis (Fig. 4). With increasing deposition time, the contact angle increases and levels off at 165°. Spherical droplets of water are exhibited on the as-prepared coatings with deposition times of 20 minutes, 25 minutes, and 30 minutes. However, water contact hysteresis is different. The coatings with deposition times of 25 minutes and 30 minutes show low contact angle hysteresis of 1.6° and 0.5°, respectively.

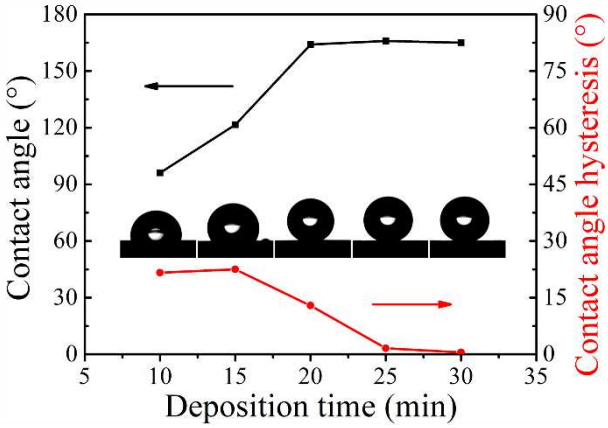

Fig. 4. Contact angle and contact angle hysteresis of titania coatings on silicon wafers after different deposition times (Insets are the water droplets on titania surfaces after different deposition times, respectively). The error limits of contact angle and contact angle hysteresis values are ~1° and ~0.5°, respectively.

The Wenzel and Cassie-Baxter models were unitized to explicate the hydrophobicity of the as-prepared coatings. The complete liquid-solid contact state is explained by Wenzel model, in which the droplets impregnate the surface. The hydrophobic titania surfaces fabricated with deposition times of 10, 15, 20 minutes with high contact angle hysteresis are in the Wenzel state. The contact angles on titania surfaces are increased with roughness, which is induced by the increased deposition times. The Wenzel state mainly occurs with moderate surface roughness, where liquid droplet can impregnate into the surface.

The high contact angle and low contact angle hysteresis of the superhydrophobic titania surface fabricated with deposition time of 25, 30 minutes indicate that they are in the Cassie-Baxter state. Direct contact between water droplets and the solid surface is prevented by an air layer, leading to the increase of air-liquid interface area. It reveals that the liquid droplet contacts with the top of asperities and air bubbles are entrapped in the rough structure, leading to a decrease of solid-liquid interface and increase of air-liquid interface. This phenomenon mainly occurs with a high surface roughness or hierarchical structures, where the air layer captured by the structures successfully blocks the penetration of water into the surface. Consequently, the contact angle hysteresis of superhydrophobic titania surface is low, indicating that the liquid droplet easily rolls off upon these surfaces.

The results suggest that the superhydrophobicity of coatings are attributed to the modification of PFTEOS and their hierarchical structures. The superhydrophobic behavior correlates well with the SEM. With increase of deposition times, the surface roughness increases, leading to a more complex hierarchical structure. The complex hierarchical structure can effectively entrap an air layer to prevent the direct contact between liquid and solid surface. Coatings with the deposition time of 30 minutes shows a high water contact angle and a low contact angle hysteresis, indicating the formation of a stable air layer.

3.3 Titania Coatings on Different Substrates

The sol-gel deposition process can be applied to various substrates. Hydroxyl groups need to be introduced onto substrate surfaces to enable chemisorption and hydrolysis process. This can be achieved by different methods depending on the materials. Hydroxyl groups on some substrates, such as stainless steel [36], silicon wafers and glass substrates [42], can be generated by a piranha solution. UV irradiation has been known to generate hydroxyl groups on aluminum substrates by the following reactions: $3O_2 + h\nu = 2O_3$, $O_3+H_2O+h\nu=O_2+H_2O_2$, and $H_2O_2+h\nu=2\bullet OH$. The enrichment of hydroxyl groups results in more hydrophilic surfaces, as the static water contact angles of the surfaces decrease (Fig. 5). The consecutive build-up of titania particles on stainless steel, glass substrates, and aluminum substrates are visible in SEM images (Supported Information Fig. S1). Titania particle layers on stainless steel and aluminum substrates are formed with three deposition cycles, and each cycle is 30 minutes. Titania particle layers on glass substrate is formed within 30 minutes. It is obvious that a compact titania layer is formed on aluminum substrates. Meanwhile, similar to the titania coatings on silicon wafers, titania coatings on stainless steel, glass substrates, and aluminum substrates show a significantly high contact angle, comparing to the untreated reference samples (Fig. 5). The introduction of titania coatings changes the wettability for all the samples and shows a low contact angle hysteresis, indicating the successful fabrication on various materials. The presented method improves the simplicity and versatility of accessible substrate materials, shapes and sizes.

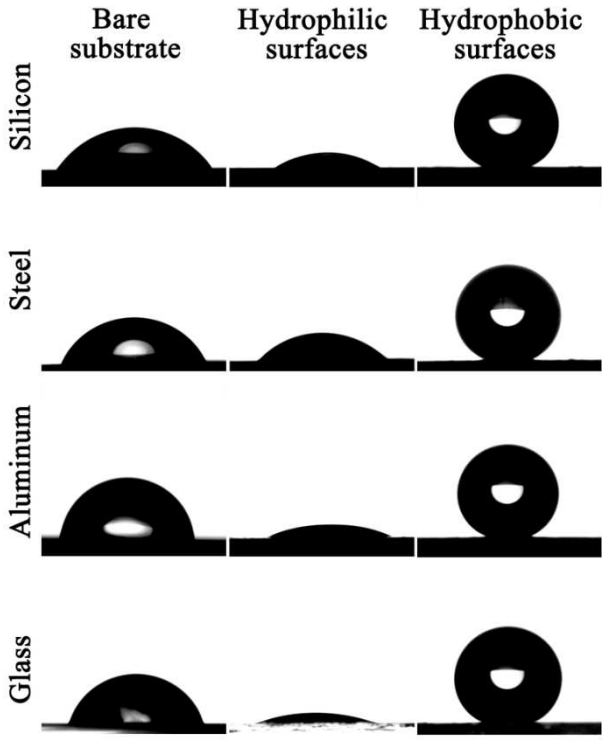

Fig. 5. Initial wettability of silicon, steel, aluminum and glass bare substrates. Hydrophilicity of silicon, steel, aluminum and glass substrates with introduced hydroxyl groups. Hydrophobicity of silicon, steel, aluminum and glass substrates with titania coatings with grafted PFTEOS molecules, indicating the substrate-independency of the coating process.

3.4 Stability of Superhydrophobic Titania Coatings

The superhydrophobic surfaces, as engineering materials, their stability over a wide pH-range is significant for their practical applications. In general, antiwetting performance of superhydrophobic surfaces will be weakened when they contact with acid/ alkaline media [24, 27]. Since both acid and alkaline solutions could react with aluminum to decrease their contact angles, the antiwetting performance towards acid and alkaline solutions of the as-prepared superhydrophobic titania surfaces on aluminum substrates were studied in detail. The superhydrophobic titania surfaces on aluminum substrates show superior resistance towards HCl solution with pH=1 and NaOH solution with pH=14. The droplets of HCl solution (pH=1) on the superhydrophobic aluminum surface can keep a spherelike shape for at least 30 minutes. And the droplets can quickly and easily roll off from the surfaces without any trace. However, when the HCl solution (pH=1) is placed on aluminum substrate, it stays on the surface and induces corrosion. The acid solution almost has no effects on the

superhydrophobic titania surface. The results demonstrate that the surface has a high stability towards chemical solutions. The contact angles as a function of pH on the superhydrophobic titania surfaces are shown in Fig. 6a. There is just a slight decrease in contact angle of the superhydrophobic surfaces when the pH values are varied from 7 to 1, or 7 to 14 and the decrease in contact angle of alkaline solution is obvious than that of the acid solution. The contact angles remain above 150° for acid and alkaline solutions on the superhydrophobic titania surfaces.

The relationship between contact angle water and volume of droplets on titania surfaces on aluminum substrates was investigated. 10-20 μL droplets were placed on the superhydrophobic titania surfaces. Amazingly, the water contact angles on the superhydrophobic titania surfaces remain constant at ~165° (Fig. 6b). Spherical water droplets of 10, 15, and 20 μL show the contact angles of 166.7°, 166.1°, and 164.5°, respectively. It clearly reveals that the as-prepared surfaces exhibit wonderful superhydrophobicity regardless of the droplet volume. Although, the resistance towards HCl/NaOH solution is weaker. The as-prepared surface still shows contact angles higher than 150°, indicating good resistance toward HCl solution with pH=1 and NaOH solution with pH=14 regardless of the droplet volume.

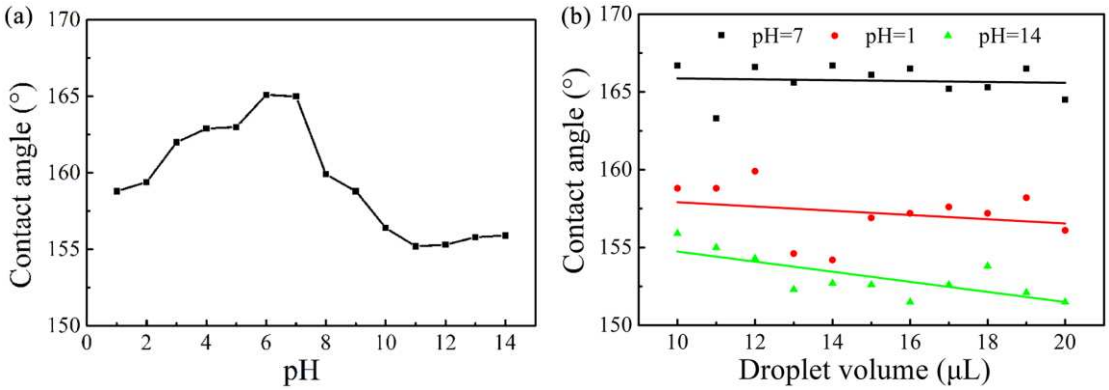

Fig. 6. Contact angles as functions of pH values (a) and contact angles as functions of droplet volume (b) on superhydrophobic surfaces on aluminum substrates. The error limits of contact angle values are ~1°.

3.5 MD simulations for hydrophobic analysis

MD simulations were used to investigate the wettability of the Al (111) and fluorinated surfaces. The fluorinated surfaces were used to simulate the as-prepared surface since PFTEOS molecules are the main surface component (Fig. 2). In the equilibrated

configuration of TiO_2 (101) crystal surface and $CF_3(CF_2)_7CH_2CH_2Si(OH)_3$ system in ethanol solution, it shows that all the alkyl chains in $CF_3(CF_2)_7CH_2CH_2Si(OH)_3$ remain in an approximately vertical state and far from the surface (Fig. S2). Therefore, we speculated the $CF_3(CF_2)_7CH_2CH_2Si(OH)_3$ molecules were in vertical state and put the $CF_3(CF_2)_7CH_2CH_2Si(OH)_3$ molecules to stay vertical and then optimize to construct the simulated fluorinated surface.

The energy curves for the simulation system between a HCl solution, water, or NaOH solution and Al (111) or simulated fluorinated surface are stable and no strong fluctuation occurs after 50 ps simulation, indicating that the system achieves an equilibrium (Fig. S3). The droplets of HCl solution, water, and NaOH solution are spread and covered on Al (111) surface, resulting in smooth liquid layers (Fig. S4). While, the droplets on the simulated fluorinated surface still kept relatively hemispherical shapes (Fig. S4). The interfacial interactions were further investigated by different liquid layers on Al (111) and simulated fluorinated surface. Water molecules formed a compact hydrated layer on Al (111) surface (Fig. 7a). The strongest peak in the water density curve is located at 3.10 Å from the Al (111) surface with a highest density of 3.97 g/mL and the strongest peak in the $H3O^+$ relative concentration is at 2.82 Å in a HCl solution system. However, the strongest peak in the water density curve is located at 2.93 Å from Al (111) surface with a highest density of 4.51 g/mL in water system. It is obvious the peak intensity of water density curve is lower than that without $H3O^+$ ions due to replacement of $H3O^+$ ions. The results indicate that $H3O^+$ ions prefer to adsorb onto aluminum surface. A similar phenomenon is also occurred on the Al (111) surface in a NaOH solution system. The results indicate Al (111) surface is hydrophilic, and hydrogen or hydroxyl ions are prone to adsorb on Al (111) surface than water molecules. However, the peaks of the first hydrated layer on the simulated fluorinated surface are broaden with lower intensity, confirming the lower attractive force between surface and water molecules. The lower interaction with water molecules usually results in hydrophobicity. Interestingly, the antiwetting performance of the fluorinated surface seems to be slightly weaken in a NaOH solution, since there are more water molecules in the first hydrated layer.

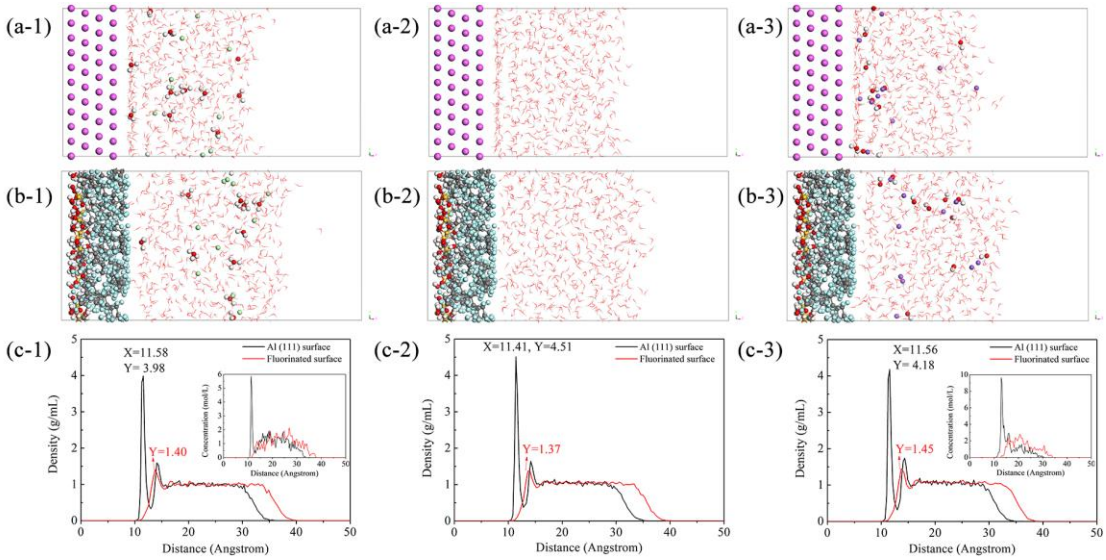

Fig. 7 Snapshots of the MD simulation about the interaction between a HCl solution (-1), water (-2), or NaOH solution (-3) and Al (111) (a) or simulated fluorinated surface (b) at equilibrium configuration. (c): Distribution of water molecules and ions on Al (111) and simulated fluorinated surfaces. The atom coloring scheme is Al, magenta; O, red; H, light gray; Cl, green; Na, purple; C, gray; F, light cyan; Si, yellow.

The antiwetting performance of the fluorinated surface was further investigated by the dynamic behavior of molecules on its surface. The dynamic properties of the water molecules in the first hydrated layer on the simulated fluorinated surface were expressed by the mean square displacement (MSD) [29]. The diffusion coefficient of the water molecules in the first hydrated layer can be represented by the slope of MSD curve. A smaller slope of MSD indicates a weaker diffusion and slower mobility. The mobility of hydrated water molecules in NaOH solution on the simulated fluorinated surface is found to be slowest, compared to the water molecules in HCl solution and neutral solution (Fig. 8). The mobility of the hydrated water molecules in NaOH solution is limited, indicating that the interaction between water molecules in NaOH solution and the simulated fluorinated surface is increased.

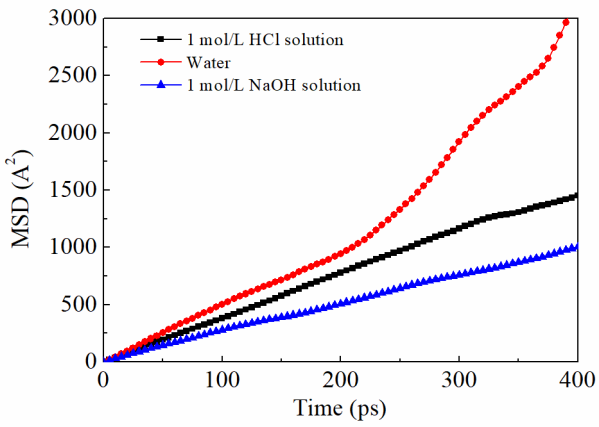

Fig. 8 Mean square displacement (MSDs) of hydrated water molecules. The water molecules for analyses are in the first hydrated layer on the simulated fluorinated surface.

The interaction between the water molecules and the Al (111) or simulated fluorinated surfaces was obtained by considering the interaction energy, which was calculated by the Equation (1):

$$\Delta E = {(E_{total} - E_{surface} - E_{solution})}/{S} \qquad (1)$$

In this equation, ΔE is the interaction energy between the different solutions and the Al (111) or simulated fluorinated surfaces. E_{total}, $E_{surface}$, $E_{solution}$ are the energy of the total system, surface, and solution, respectively. S is the area of contact surface. A more favorable interaction occurred with a more negative interaction energy. It is obvious that the interaction energies of Al surface-solution systems are much higher than that of fluorinated surface-solution systems, indicating that the solution prefers to adsorb on Al surface rather than the fluorinated surface. Van der Waals interaction is responsible for the hydrophilicity of the Al (111) surface. Moreover, the interaction energies of Al surface- HCl solution system and Al surface-NaOH solution system are a little lower than that of Al surface-water system (-0.361 and -0.367 versus -0.358 kcal/mol/Å^2). While, the interaction energies of fluorinated surface-HCl solution system and fluorinated surface-NaOH solution system are more negative than that of fluorinated surface-water system (-0.071 and -0.186 versus -0.070 kcal/mol/Å^2). The difference in interaction energies is directly related to the electrostatic interaction. In the alkaline solution, the electrostatic interaction increases to -0.126 kcal/mol/Å^2, which is much more negative than -0.012 kcal/mol/Å^2 in water, which maybe cause by the adsorption of OH^- ions and water molecules. Both electrostatic and van der Waals interactions take

place in the interaction between fluorinated surface-solution systems. Among these, the electrostatic interaction leads to the slight decrease in hydrophobicity of fluorinated surface in an alkaline solution. The simulation results agree with the experiment results (Fig. 6), where the contact angles are slightly decreased towards alkaline solution. This study clarified the hydrophilicity of Al (111) surface and hydrophobicity of fluorinated surfaces by studying the behavior of water molecules at the atomic/molecular level for the first time. It clearly points out that the hydrophobicity of fluorinated surfaces is obtain by decreasing the van der Waals interaction with water molecules. The slight decrease in hydrophobicity of fluorinated surfaces in an alkaline solution is due to the increased electrostatic interaction.

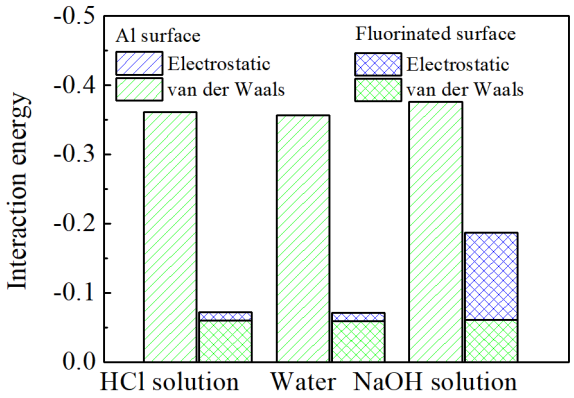

Fig. 9 Interaction energy between different solution and the Al (111) or simulated fluorinated surfaces (Unit: kcal/mol/Å^2).

4. Conclusions

This study has presented an easy and effective one-step process to introduce fluorinated coatings to a series of materials, including metals, glass, and silicon wafer. The repellency towards water was increased with the increasing deposition cycles and deposition time. The hydrophilicity of substrate surfaces and hydrophobicity of as-prepared fluorinated surfaces were revealed by MD simulations at molecular level. The MD simulations indicated that substrate surfaces preferred to adsorb hydrogen or hydroxyl ions rather than water molecules. However, there were much fewer hydrated water molecules on the as-prepared fluorinated surface, confirming their antiwetting properties. The electrostatic interaction led to a slight decrease in hydrophobicity of the fluorinated surface in an alkaline solution. The study would give insights into fabricating superhydrophobic surfaces on different substrates simply and feasibly by a one-step process and provide a further understanding of the wettability of fluorinated

superhydrophobic surface.

Acknowledgments

This work was supported by National Natural Science Foundation of China (Grant No. 52001238 and 52071246), and the International Postdoctoral Exchange Fellowship Program (Grant No. 20190060).

References

[1] L. Jiang, Y. Zhao, J. Zhai, A lotus-leaf-like superhydrophobic surface: A porous microsphere/nanofiber composite film prepared by electrohydrodynamics, Angew. Chem. Int. Ed. 43 (2004) 4338-4341.

[2] S. Ma, Q. Ye, X. Pei, D. Wang, F. Zhou, Antifouling on gecko's feet inspired fibrillar surfaces: evolving from land to marine and from liquid repellency to algae resistance, Adv. Mater. Interfaces 2 (2015) 1500257.

[3] C. Schlaich, L. Yu, L.C. Camacho, Q. Wei, R. Haag, Fluorine-free superwetting systems: construction of environmentally friendly superhydrophilic, superhydrophobic, and slippery surfaces on various substrates, Poly. Chem. 7 (2016) 7446-7454.

[4] X. Zhao, D.S. Park, J. Choi, S. Park, S.A. Soper, M.C. Murphy, Robust, transparent, superhydrophobic coatings using novel hydrophobic/hydrophilic dual-sized silica particles, J. Colloid Interface Sci. 574 (2020) 347-354.

[5] S.S. Latthe, R.S. Sutar, V.S. Kodag, A.K. Bhosale, A.M. Kumar, K. Kumar Sadasivuni, R. Xing, S. Liu, Self – cleaning superhydrophobic coatings: Potential industrial applications, Prog. Org. Coat. 128 (2019) 52-58.

[6] A.K. Sasmal, C. Mondal, A.K. Sinha, S.S. Gauri, J. Pal, T. Aditya, M. Ganguly, S. Dey, T. Pal, Fabrication of superhydrophobic copper surface on various substrates for roll-off, self-cleaning, and water/oil separation, ACS Appl. Mater. Interfaces 6 (2014) 22034-22043.

[7] P.G. Pawar, R. Xing, R.C. Kambale, A.M. Kumar, S. Liu, S.S. Latthe, Polystyrene assisted superhydrophobic silica coatings with surface protection and self-cleaning approach, Prog. Org. Coat. 105 (2017) 235-244.

[8] J. Jeon, H. Jang, J. Chang, K.-S. Lee, D.R. Kim, Fabrication of micro-patterned aluminum surfaces for low ice adhesion strength, Appl. Surf. Sci. 440 (2018) 643-650.

[9] X. He, P. Cao, F. Tian, X. Bai, C. Yuan, Autoclaving-induced in-situ grown hierarchical structures for construction of superhydrophobic surfaces: A new route to fabricate antifouling coatings, Surf. Coat. Technol. 357 (2019) 180-188.

[10] W. Long, H. Li, B. Yang, N. Huang, L. Liu, Z. Gai, X. Jiang, Superhydrophobic diamond-coated Si nanowires for application of anti-biofouling', J. Mater. Sci. Technol. 48 (2020) 1-8.

[11] A.B. Radwan, A.M. Abdullah, N.A. Alnuaimi, Recent advances in corrosion resistant superhydrophobic coatings, Corros. Rev. 36 (2018) 127-153.

[12] I.O. Arukalam, C.N. Njoku, L. Yang, B. Hou, Y. Li, Inhibition of sulfate-reducing bacteria influenced corrosion on hydrophobic poly(dimethylsiloxane) coatings, J. Mater. Sci. Technol. 52 (2020) 198-206.
[13] G.D. Bixler, B. Bhushan, Fluid drag reduction and efficient self-cleaning with rice leaf and butterfly wing bioinspired surfaces, Nanoscale 5 (2013) 7685-7710.
[14] Y.F. Fu, C.Q. Yuan, X.Q. Bai, Marine drag reduction of shark skin inspired riblet surfaces, Biosurface and Biotribology 3 (2017) 11-24.
[15] V.K. Truong, H.K. Webb, E. Fadeeva, B.N. Chichkov, A.H.F. Wu, R. Lamb, J.Y. Wang, R.J. Crawford, E.P. Ivanova, Air-directed attachment of coccoid bacteria to the surface of superhydrophobic lotus-like titanium, Biofouling 28 (2012) 539-550.
[16] A.B.D. Cassie, S. Baxter, Wettability of porous surfaces, Transactions of the Faraday Society 40 (1944) 0546-0550.
[17] R. Jafari, M. Farzaneh, Fabrication of superhydrophobic nanostructured surface on aluminum alloy, Appl. Phys. A 102 (2011) 195-199.
[18] L. Feng, H. Zhang, Z. Wang, Y. Liu, Superhydrophobic aluminum alloy surface: fabrication, structure, and corrosion resistance, Colloids Surf. A 441 (2014) 319-325.
[19] B.S. Yilbas, M. Khaled, N. Abu-Dheir, N. Aqeeli, S.Z. Furquan, Laser texturing of alumina surface for improved hydrophobicity, Appl. Surf. Sci. 286 (2013) 161-170.
[20] S.S. Latthe, H. Imai, V. Ganesan, A.V. Rao, Superhydrophobic silica films by sol–gel co-precursor method, Appl. Surf. Sci. 256 (2009) 217-222.
[21] X. Zhou, Y.-Y. Lee, K.S.L. Chong, C. He, Superhydrophobic and slippery liquid-infused porous surfaces formed by the self-assembly of a hybrid ABC triblock copolymer and their antifouling performance, J. Mater. Chem. B 6 (2018) 440-448.
[22] X. Gao, Z. Guo, Mechanical stability, corrosion resistance of superhydrophobic steel and repairable durability of its slippery surface, J. Colloid Interface Sci. 512 (2018) 239-248.
[23] C. Du, X. He, F. Tian, X. Bai, C. Yuan, Preparation of superhydrophobic steel surfaces with chemical stability and corrosion, Coatings 9 (2019) 398.
[24] S. Peng, X. Yang, D. Tian, W. Deng, Chemically stable and mechanically durable superamphiphobic aluminum surface with a micro/nanoscale binary structure, ACS Appl. Mater. Interfaces 6 (2014) 15188-15197.
[25] X.-F. Zhang, Y.-Q. Chen, J.-M. Hu, Robust superhydrophobic SiO2/polydimethylsiloxane films coated on mild steel for corrosion protection, Corros. Sci. 166 (2020).
[26] N. Saleema, D.K. Sarkar, R.W. Paynter, X.-G. Chen, Superhydrophobic aluminum alloy surfaces by a novel one-step process, ACS Appl. Mater. Interfaces 2 (2010) 2500-2502.
[27] B. Zhang, J. Li, X. Zhao, X. Hu, L. Yang, N. Wang, Y. Li, B. Hou, Biomimetic one step fabrication of manganese stearate superhydrophobic surface as an efficient barrier against marine corrosion and Chlorella vulgaris-induced

biofouling, Chem. Eng. J. 306 (2016) 441-451.
[28] T. Li, J. Li, H. Lin, Y. Duan, Y. Xia, Y. Jiang, H. Li, Control of wettability transition and coalescence dynamics of droplets on the surface via mechanical vibration: A molecular simulation exploration, Appl. Surf. Sci. 473 (2019) 393-400.
[29] R. Zhang, Y. Xing, Y. Xia, J. Luo, J. Tan, G. Rong, X. Gui, New insight into surface wetting of coal with varying coalification degree: An experimental and molecular dynamics simulation study, Appl. Surf. Sci. 511 (2020) 145610.
[30] S. Li, Y. Liu, Z. Zheng, X. Liu, H. Huang, Z. Han, L. Ren, Biomimetic robust superhydrophobic stainless-steel surfaces with antimicrobial activity and molecular dynamics simulation, Chem. Eng. J. 372 (2019) 852-861.
[31] X. He, T. Lou, Z. Yang, X. Bai, C. Yuan, C. Wang, A. Neville, Lubricant-infused titania surfaces with high underwater transparency for antifouling applications: A combined experimental and molecular dynamics study, Appl. Surf. Sci. 543 (2021) 148848.
[32] L. Guo, G.H. Tang, S. Kumar, Droplet morphology and mobility on lubricant-impregnated surfaces: a molecular dynamics study, Langmuir 35 (2019) 16377-16387.
[33] C. Li, T. Zhang, X. Ji, Z. Wang, S. Sun, S. Hu, Effect of Ca^{2+} /Mg^{2+} on the stability of the foam system stabilized by an anionic surfactant: A molecular dynamics study, Colloid Surf. A 489 (2016) 423-432.
[34] Y.N. Ahn, S.H. Lee, S.Y. Oh, Adsorption characteristics of silane-functionalized perfluoropolyether on hydroxylated glassy silica surfaces: A multiscale approach, Appl. Surf. Sci. 496 (2019) 143699.
[35] Z. Shang, X. Zhang, Theoretical study on the interactions between silica and the products of 3-mercaptopropyltriethoxysilane (MPTS) with different hydrolysis degrees, Appl. Surf. Sci. 502 (2020) 143853.
[36] S.J. Yuan, S.O. Pehkonen, Y.P. Ting, K.G. Neoh, E.T. Kang, Inorganic-organic hybrid coatings on stainless steel by layer-by-layer deposition and surface-initiated atom-transfer-radical polymerization for combating biocorrosion, ACS Appl. Mater. Interfaces 1 (2009) 640-652.
[37] X. He, F. Tian, X. Bai, C. Yuan, C. Wang, A. Neville, Biomimetic lubricant-infused titania nanoparticle surfaces via layer-by-layer deposition to control biofouling, Appl. Surf. Sci. 515 (2020) 146064.
[38] H. Zhang, X. Lv, Y. Li, Y. Wang, J. Li, P25-graphene composite as a high performance photocatalyst, ACS Nano 4 (2009) 380-386.
[39] Y. Sun, L. Wang, Y. Gao, D. Guo, Preparation of stable superamphiphobic surfaces on Ti-6Al-4V substrates by one-step anodization, Appl. Surf. Sci. 324 (2015) 825-830.
[40] J. Yin, M.L. Mei, Q. Li, R. Xia, Z. Zhang, C.H. Chu, Self-cleaning and antibiofouling enamel surface by slippery liquid-infused technique, Sci. Rep. 6 (2016) 25924.
[41] X. Rao, C. Guyon, S. Ognier, B. Da Silva, C. Chu, M. Tatoulian, A.A. Hassan, High density gold nanoparticles immobilized on surface via plasma deposited

APTES film for decomposing organic compounds in microchannels, Appl. Surf. Sci. 439 (2018) 272-281.

[42] S. Sunny, N. Vogel, C. Howell, T.L. Vu, J. Aizenberg, Lubricant-infused nanoparticulate coatings assembled by layer-by-layer deposition, Adv. Funct. Mater. 24 (2014) 6658-6667.